Bulletin of the Seismological Society of America, Vol. 96, No. 1, pp. 33–47, February 2006, doi: 10.1785/0120050094

Ⓔ

Stream Channel Offset and Late Holocene Slip Rate of the San Andreas Fault at the Van Matre Ranch Site, Carrizo Plain, California

by Gabriela R. Noriega, J Ramón Arrowsmith, Lisa B. Grant, and Jeri J. Young

Abstract Sets of well-preserved channels offset across the San Andreas fault (SAF) at the Van Matre Ranch (VMR) site in the northwestern Elkhorn Hills area of the Carrizo Plain offer the opportunity to measure slip rate and examine geomorphic development of the channels. The fault zone and offset channels were exposed by excavation in one fault-perpendicular and five fault-parallel trenches. The geomorphology and stratigraphy in the channels reveal a record of filling by fluvial sedimentation, lateral colluviation, and pedogenesis. The buried thalweg of the currently active channel is offset 24.8 ± 1 m, while the geomorphic channel is offset approximately 27.6 ± 1 m. Seventeen samples were collected from channel margin deposits for ^{14}C dating. An OxCal model of the radiocarbon dates with stratigraphic control suggests that the oldest date for channel incision was ~A.D. 1160. Minimum and maximum slip rates ranging from 29.3 to 35.6 mm/yr are derived from different assumptions about the timing of channel incision and offset. The resulting slip rates at VMR agree well with the late-Holocene slip rate of 33.9 ± 2.9 mm/yr at Wallace Creek, approximately 18 km to the northwest, and imply that within measurement uncertainty the 30–37 mm/yr velocity gradient across the SAF from decadal timescale geodetic measurements is accommodated across the several-meter-wide SAF zone at VMR over the last millennium.

Online material: Supplemental unit descriptions, trench logs, and ^{14}C data.

Introduction

The southern San Andreas fault (SAF) south of the creeping section is recognized as southern California's most likely source of future great earthquakes (Figs. 1 and 2; Working Group on California Earthquake Probabilities [WGCEP], 1988, 1995). The Carrizo Plain (Figs. 1 and 2) has been one of the most productive sections of the SAF for paleoseismic research, yielding late-Pleistocene and mid-Holocene slip rates (Sieh and Jahns, 1984), slip-per-event measurements for the last six ruptures Grant and Sieh, 1993; Grant and Donnellan, 1994; (Liu *et al.,* 2004), and dates of the last five major earthquakes (Grant and Sieh, 1994; Sims, 1994). Additionally, from multiple measurements of slip in the most recent A.D. 1857 earthquake (Sieh, 1978; Grant and Sieh, 1993; Grant and Donnellan, 1994), it appears that the SAF sustained maximum slip in the Carrizo Plain. This section of the fault may control the occurrence of great earthquakes along the southern SAF (Sieh and Jahns, 1984; Wells and Coppersmith, 1984) through repetition of similar large events with relatively long recurrence intervals, although some paleoseismic data suggest variable rupture magnitudes and irregular recurrence intervals (Grant and Sieh, 1994; Grant, 1996). These interpretations have different implications for seismic hazard assessment and fault models.

Slip rate is an essential input parameter for either time-dependent or static calculations of seismic hazard on the SAF. Argus and Gordon (2001) determined that 39 ± 2 mm/yr of relative motion between the Pacific and North American plates is accommodated along the SAF and central California Coast Ranges. The difference between the SAF slip rate and this regional slip budget will indicate the degree of localization of that deformation and the potential for other active seismogenic structures in the Coast Ranges. Sieh and Jahns (1984) reported a slip rate of 33.9 ± 2.9 mm/yr for the SAF in the Carrizo Plain over the last 3700 years, in agreement with their late Pleistocene rate of ~36 mm/yr. Our study provides a latest Holocene slip rate for comparison with late-Pleistocene, mid-Holocene, and geodetic measurements of deformation. The slip rate is derived from the measurement and dating of offset stream channels. It also provides an opportunity to characterize evolution of the offset stream channels, and thus develop understanding of their tectonic and geomorphic development.

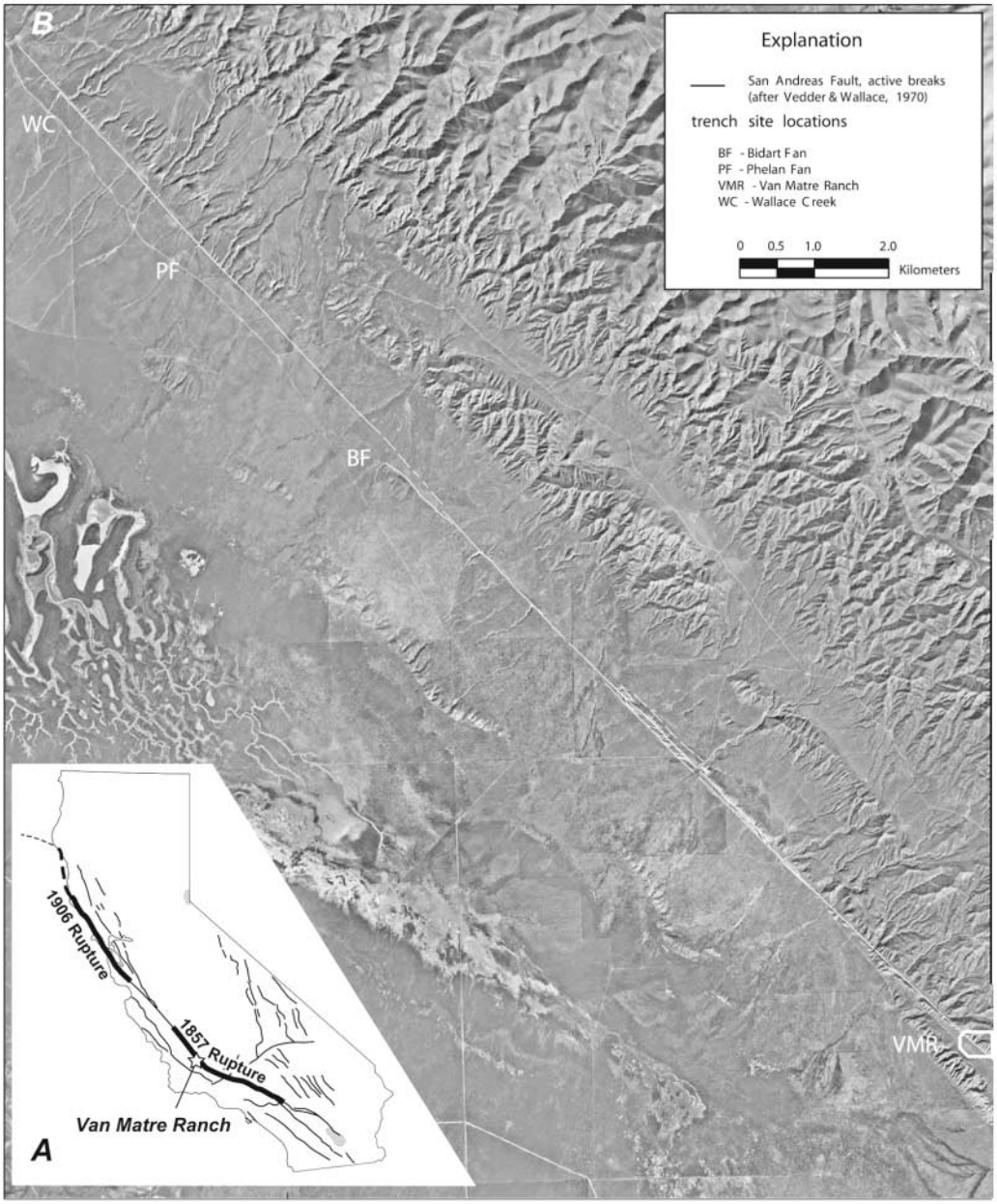

Figure 1. (A) Major historic ruptures along the SAF (modified from Allen, 1968) showing location of VMR site in northwestern portion of SAF that ruptured in the 1857 earthquake. (B) Aerial photograph mosaic of Carrizo Plain showing active fault trace observations from Vedder and Wallace (1970) as well as locations of Bidart Fan (BF), Phelan Fan (PF), Wallace Creek (WC), and Van Matre Ranch (VMR) paleoseismic sites. Polygon at VMR shows the location of aerial photography in Figure 3.

Site Location and History

The Carrizo Plain is an arid-to-semiarid closed basin situated at an elevation of about 580 m. It is physiographically separate from the San Joaquin basin to the northeast and the Cuyama Valley to the southwest by the intervening Temblor and Caliente Ranges respectively (Figs. 1 and 2). The Van Matre Ranch (VMR) site is in the southern Carrizo Plain (Fig. 1), approximately 18 km southeast of the multiple paleoseismic sites at Wallace Creek (Sieh and Jahns, 1984; Liu, 2003; Liu *et al.*, 2004), Phelan Creeks (Sims, 1994), Phelan fan (Grant and Sieh, 1993), and Bidart fan (Grant and Sieh, 1994). The geomorphic manifestation of repeated ground rupture is evident in the well-preserved series of beheaded and abandoned stream channels at VMR (Figs. 3–5). Prior to this study Prentice and Sieh (1989) and Sims *et al.*

(*text continues on page 38*)

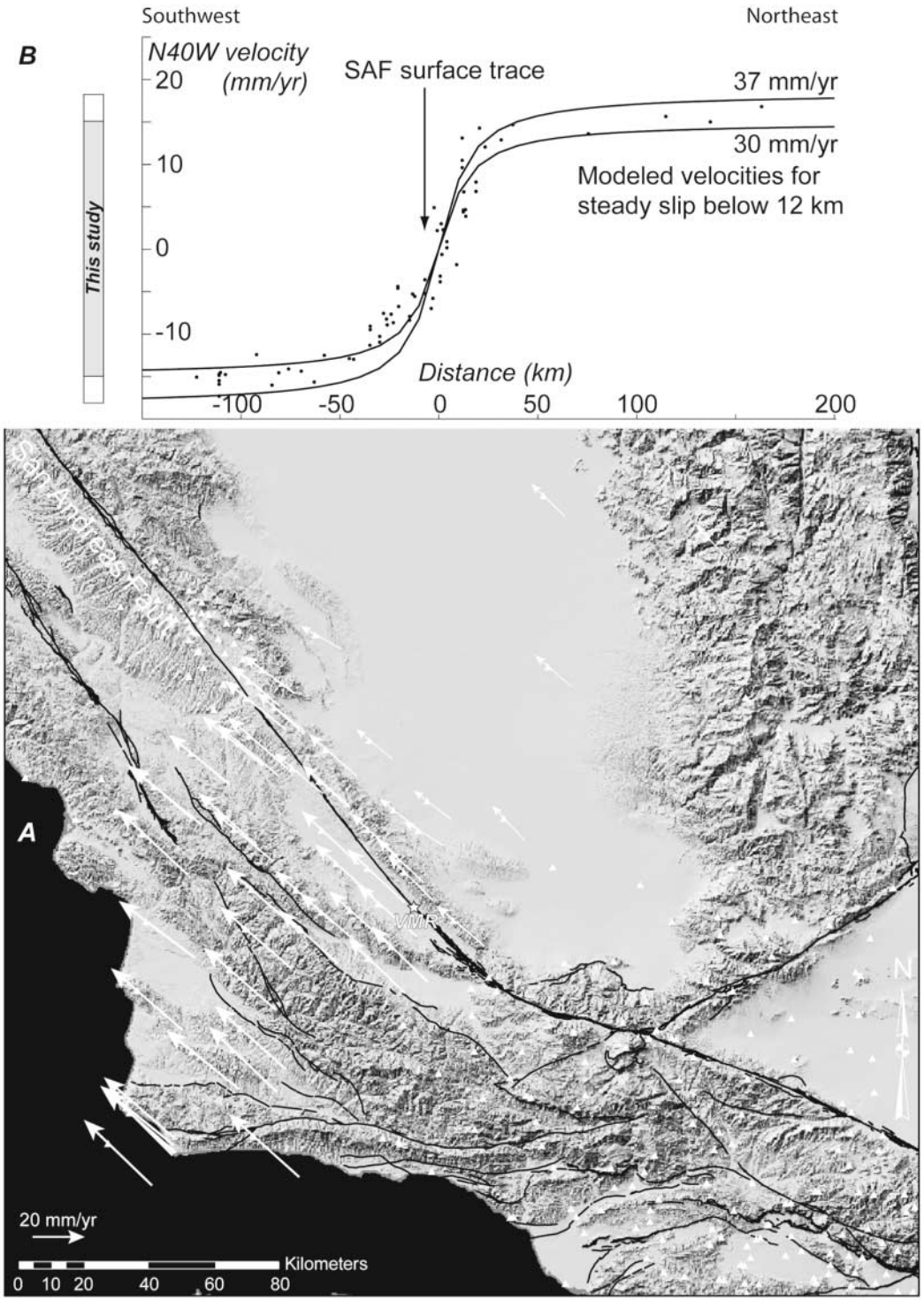

Figure 2. (A) Shaded relief, active faults (modified from Quaternary Fault and Fold Database for the United States, http://qfaults.cr.usgs.gov/) of southern California and selected site velocities from the Southern California Earthquake Center Crustal Motion Map (CMM3; Shen *et al.*, 2003). White triangles show all CMM3 sites in the region, and those we selected from the group have velocities shown by arrows (note the velocity scale at the bottom). The maximum velocity uncertainty is 4.6 mm/yr, but the maximum in the N40°W direction is 1.6 mm/yr. The clear velocity gradient across the SAF is shown in (B). The location of the VMR site is indicated by the star. (B) The N40°W parallel component of the selected CMM3 velocities is plotted with respect to distance from the SAF and relative to 0 mm/yr at the SAF. The two curves show modeled velocities for steady interseismic slip below 12 km and bracket most of the observed motion. At left, the slip-rate estimate from our study of 35.4 ± 8.8 mm/yr with uncertainties indicated by the white boxes is drawn for comparison.

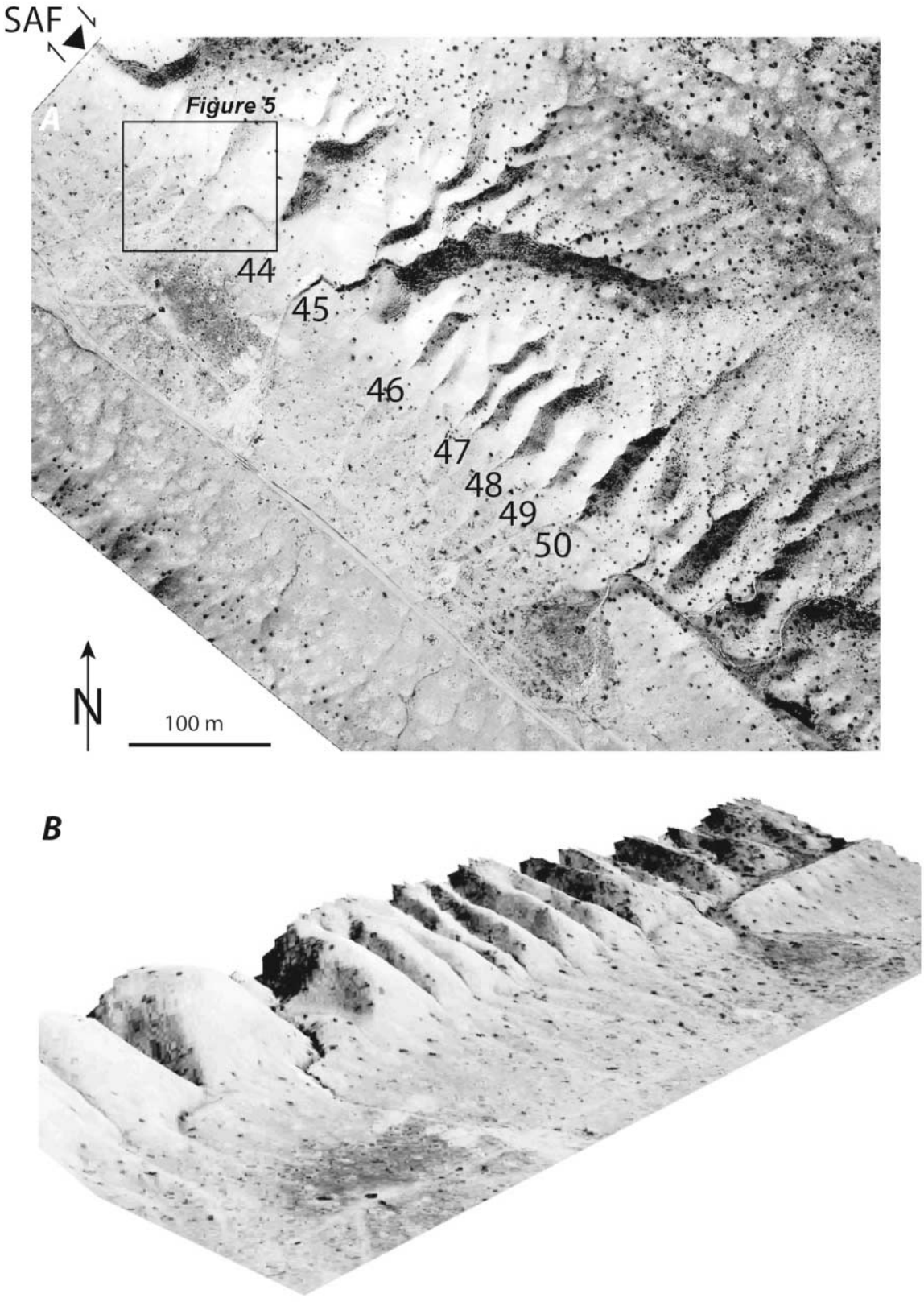

Figure 3. (A) Rectified aerial photograph (9 March 1991; original scale 1:3,000) showing the clear traces of the SAF at the VMR site (see Fig. 1 for location) with numerous small offsets (those studied by Sieh [1978] are shown with corresponding numbers). In this study, we focused on channel 44 (the outline of Fig. 5 is shown by the black rectangle). (B) Oblique view to the east-southeast of aerial photo draped over photogrammetrically produced and digitized elevation data.

Figure 4. (A) Overview to the west of the VMR site. The arrow shows the view direction of B. (B) View southeast along the SAF showing the upstream channel segment at the study site (behind person on left in B) leaving the upland watershed, slightly dammed by the shutter ridge to the right, and then the offset channel segment traversing the view under the nearer person and turning southwest just outside the view to the right. Trench T2 was dug parallel to the SAF and across the upstream channel mouth approximately where the person on the left crouches, and T3 was dug perpendicular to T2 up onto the shutter ridge. Compare with Figure 5.

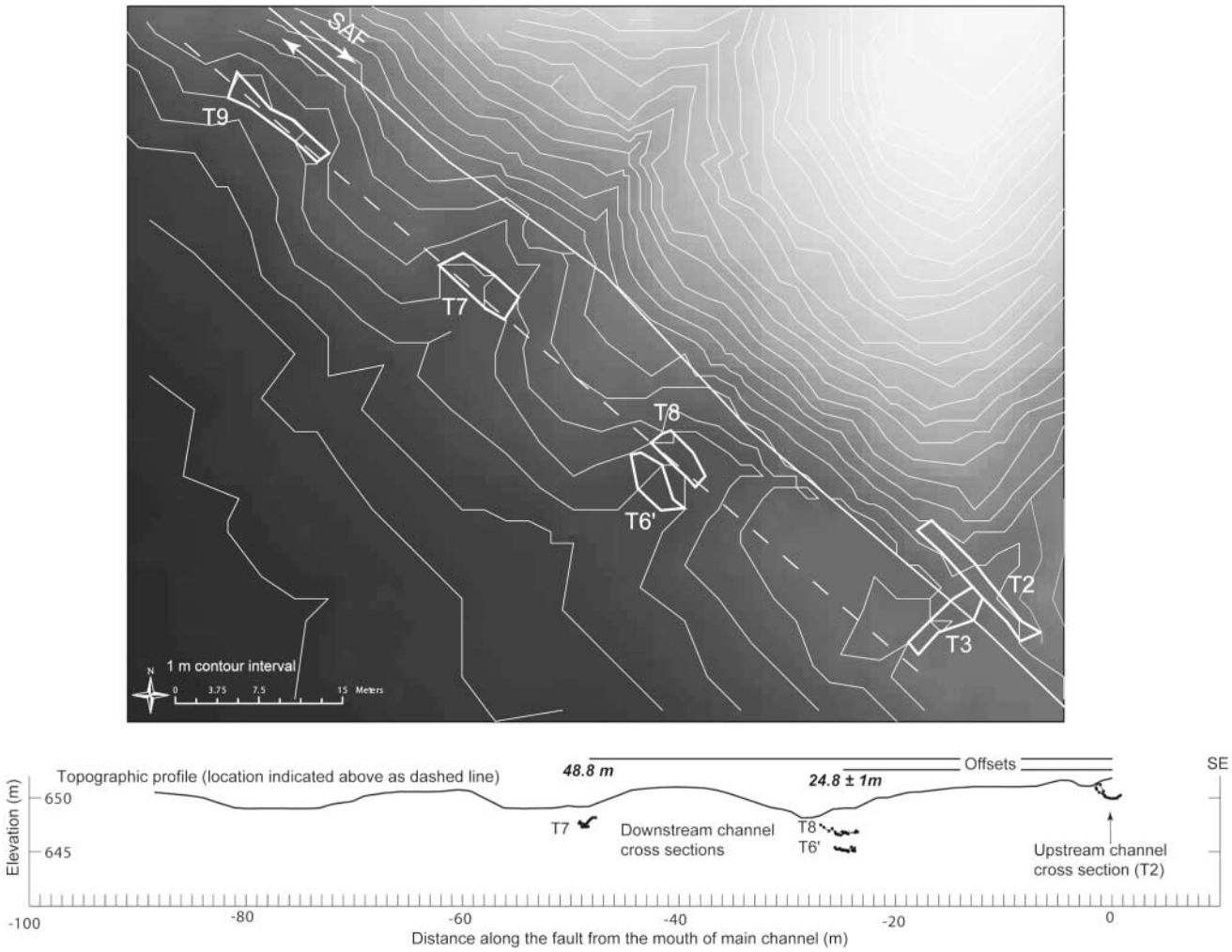

Figure 5. Topographic map of the study site with 1-m contour interval. Channels once connected to the main channel (southeast) have been offset as the three beheaded channels to the northwest. Our trench excavations exposed offset channels in T2, T3, T8, T6′, and T7. The T7 channel has subsequently captured the small drainage immediately above it. The cross section below shows the topographic profile through the beheaded channels (dashed line on map) and the projected channel cross sections exposed and surveyed in the excavations. Note that the offsets determined by matching the channels defined in the trenches are different than those determined just from the offset geomorphology. Trench locations (closed polygons) are mapped from survey data.

(1993) conducted reconnaissance investigations of VMR geomorphology and stratigraphy.

This study focuses on offset channel "gully #44" as reported by Sieh (1977, 1978, 1979; Figs. 3 and 5) and investigated by Sims *et al.* (1993). Sieh documented sites along the SAF where slip from the A.D. 1857 earthquake was well preserved, including VMR. He measured several offset channels numbered 44–50 and postulated that they were formed by 8 ± 0.5 m displacement in 1857, and two prior earthquakes with 7.5 ± 1 m and 10 ± 1 m slip (Fig. 3; Sieh, 1978, 1979).

Methodology

Trenches were located and excavated based on data from Sims *et al.* (1993) and Prentice and Sieh (1989). Trenches T2 and T3 (Fig. 5) were re-excavations of older trenches. An attempt to re-excavate trench 6 of Sims *et al.* (1993) was unsuccessful. The resulting trench, T6′, is close to T6. Three new trenches (T7, T8, and T9) were also excavated. Trenches excavated in 2004 are labeled T2, T3, T6′, T7, T8, and T9 and mapped along with the SAF (Fig. 5). T2 was excavated on the northeast side of the fault and upstream of the offset channel. T3 is a fault-perpendicular trench excavated for accurate fault location and investigation of

surface-rupturing events. T6′, T7, T8, and T9 were all excavated on the southwest side of the fault and provide exposures for offset measurements.

Trenches were excavated with a backhoe and supported by hydraulic shoring. The trenches were logged at a scale of 1:25 and the thalwegs were surveyed for spatial control and precise offset measurement. Exposures of the trench walls were also recorded by mosaic photography.

Over 1400 surveyed points define the topography at the site (see Fig. 5). Channels once connected to the main channel (southeast) have been offset to the three beheaded channels to the northwest. Our excavations exposed offset channels in trenches T2, T3, T8, T6′, and T7. The T7 channel has subsequently captured the small drainage immediately above it. Topographic survey data collected during this project were used to tie all the trenches into the same coordinate system. We also combined new data with preexisting data (Sims *et al.*, 1993) to produce the topographic map shown in Figure 5 and used them in our offset calculations (see following sections). In addition, we surveyed all major contacts exposed in the trench walls. Survey data were adjusted from the local datum to an absolute Universal Transverse Mercator (UTM) grid projection and the elevation fixed relative to sea level. Absolute location and elevation accuracy are only several meters (handheld GPS), but the internal precision of the survey is at the centimeter level.

In all of the trenches, the stratigraphic units were analyzed, identified, and logged. Sediment and soil analyses were based on unit color, rounding, sorting, clast size, matrix composition, and degree of bioturbation. Sediment analysis and interpretation was the basis for unit correlation and consequently for offset calculation. In each trench, units are numbered in hundreds corresponding to the trench number (e.g., 200 for trench T2). In trenches T2, T3, T6′, and T8, correlative units have comparable numbers such that unit 660 in T6′ correlates with unit 860 in T8, and soon. Numbers increase from oldest (e.g., unit 300) to youngest (e.g., unit 395) within a given trench. Correlations between trenches on the same side of the fault (i.e., T6′ and T8) are for the same unit. Correlations of channel units across the fault zone represent the same stratigraphic position.

Radiocarbon analysis and sample pretreatment for this project were conducted at University of California, Irvine's (UCI's) Keck carbon isotope Accelerator Mass Spectrometry Laboratory (AMS) under the supervision of J. Southon. Standards Ox-I, Ox-II, ANU (sucrose), and coal 50,000 years old were used to correct for natural graphitization and AMS fractionation. The dates extracted from the samples were calibrated using Calib 4.4 by Stuiver *et al.* (1998). Results are displayed in Table 1 and supplemental Table 1 (Ⓔ available in the electronic edition of BSSA).

Results

The stratigraphy and abundance of datable materials were favorable for measuring a late-Holocene slip rate from the channels exposed in trenches T2, T3, T6′, and T8. We exposed the correlative channel in T7, but were unable to date it. T9 exposed deformed old alluvial sediments overlain by young discontinuous channel units that were not definitively correlative with the offset channels exposed in the other trenches. The following section describes stratigraphy and results of unit correlations between trenches. Trench logs are displayed in Figure 6. (Ⓔ Additional trench logs and all stratigraphic unit descriptions are available in the electronic edition of BSSA.)

T2—Upstream Channel

T2 is a re-excavation of a trench from Sims *et al.* (1993). The trench is about 7 m long and 3 m wide and exposes relatively young channel deposits on the upstream side of the fault (Figs. 5 and 6a). The exposure geometry only preserved short portions of the outer edge equivalents of the southwest wall. Unit 200 is interpreted as local bedrock, mapped as Paso Robles Formation (QTP) on regional maps by Dibblee (1973). Along its upper contact, unit 200 shows downslope warping of units, which probably results from soil creep. Unit 200 was incised and then filled to an unknown level by channel deposits and colluvium of unit 210, both of which are bioturbated and subject to bioturbation and accumulation of pedogenic clay, carbonate, and gypsum. Unit 220 fills a channel cut into unit 200/210 with likely coeval colluvial packages of units 240 and 230. (Both units 240 and 230 are burrowed and pedogenically altered, but less so than unit 210.) Unit 250 fills a channel cut into units 240/220/230 with roughly coeval colluviation of unit 260 (and lower unit 270). Unit 260 contains numerous clasts from regional unit QTP, presumably derived from some local bedrock exposure upslope. Unit 270 at its base is probably the same as unit 260, but then overlies all other units and is in contact with the active soil horizon (Fig. 6a; Ⓔ supplemental Table 2, available in the electronic edition of BSSA).

T3—Cross-Fault Trench

T3 is a re-excavation of a portion of a trench from Sims *et al.* (1993) (Fig. 6b; Ⓔ supplemental Table 3, available in the electronic edition of BSSA). This is the only trench excavated across the SAF in 2004. Trench T3 clearly shows juxtaposed stratigraphy with unit 300 correlative with the local bedrock unit 200 from trench T2. Unit 300 is a well-lithified grayish unit with silts and thin sands alternating with clast-supported pebbles dominated by Tertiary Monterey formation–derived siltstone chips. Bedding dips to the northeast and the unit is progressively sheared to the southwest until it is completely cut out. At the base of the trench, unit 300 is juxtaposed against 310 across a zone of inferred fissure fill (unit 380). Unit 310 is a tan-beige heterogeneous unit we divided into three subunits. Unit 310A is heavily sheared pebbly silt with no clear sedimentary fabric preserved. It grades laterally into unit 310B, which is interbedded sand and silt. Units 310B and 310C are separated by a

Table 1
^{14}C Data That Apply to Slip-Rate Determination for the VMR Paleoseismic Site

Sample Code	Description	Radiocarbon Age B.P.	±	δ^{13}C	σ	Calibrated Age Ranges (A.D.)	Median Probability	Stratigraphic Unit
T6-4	wood	830	20	−18.9	1	1193–1252	1221	630
					2	1164–1262	1221	
T8-1	charcoal	615	25	−16.8	1	1303–1393	1349	860
					2	1299–1400	1349	
T8-2	charcoal	630	25	−22.2	1	1301–1390	1352	860
					2	1296–1397	1352	
T8-3	charcoal	705	20	−9.7	1	1283–1295	1288	860
					2	1274–1379	1288	
T8-4	charcoal	630	20	−18.5	1	1301–1389	1353	860
					2	1298–1395	1353	
T8-5	charcoal	675	20	−19.0	1	1288–1380	1301	860
					2	1281–1387	1301	
T8-9	charcoal	665	20	−11.4	1	1291–1384	1357	860
					2	1285–1389	1357	
T8-10	wood	675	20	−7.5	1	1288–1380	1301	860
					2	1281–1387	1301	
T8-11	charcoal	795	20	−14.6	1	1223–1264	1246	870
					2	1217–1278	1246	

All analyses are standard AMS dates from the UCI Keck Carbon Isotope facility. Calibrated dates are from Calib Radiocarbon Calibration V4.4 (2004 update of Stuiver *et al.*, 1998). Radiocarbon concentrations were given as fractions of the Modern standard, D14C, conventional radiocarbon age, and DEL14C, following the conventions of Stuiver and Polach (1977). (Ⓔ See supplemental Table 1 available in the electronic edition of BSSA.) AMS-d13C values were measured on prepared graphite using the AMS spectrometer. These can differ slightly (typically by 1–3‰) from those of the original material, if fractionation occurred during sample graphitization.

shear zone unconformably overlain (probably erosionally) by fluvial sand: unit 320. Unit 310C has preserved vertical layering in silt, but it is largely sheared and bioturbated so that the original sedimentary fabric has been obliterated. Unit 310 has some $CaCO_3$ staining, further indicating its older age relative to overlying units. Units 330, 340, and 360 represent progressively younger bioturbated and pedogenically modified units. They are silty pebbly sands that do not show any sedimentary structures. Units 350 and 370 on the northeast side of the main fault zone and 375 on the southwest represent the sedimentary fill sequences of the offset channel system that is the primary focus of this study. They are predominantly matrix-supported pebble gravels occasionally in upward fining sequences and plain and cross-laminated sands. Unit 395 is the youngest, unfaulted colluvial and fluvial unit.

T3 exposes three main shear zones, which we interpret as evidence for a minimum of three displacement events. The oldest shear zone cuts through unit 300. The southwestern shear zone cuts unit 310 and is unconformably overlain by unit 320. Unit 330 may be cut by a strand of this zone. The most recently active shear zone is capped only by unit 395 and spectacularly disrupts units 375 and 370. Not only are the units sheared, but also one or two distinctly aged fissures are filled in this zone. We infer that the youngest fissure fill formed in the 1857 earthquake.

T6′—First Downstream Channel

T6′ exposed offset channel deposits downstream of the fault (Fig. 6c; Ⓔ supplemental Table 4 and Fig. 1a, available in the electronic edition of BSSA). The local bedrock is a heavily bioturbated and pedogenically altered tan-beige set of units (610, 620, 630) with occasional (unit 620) to no preserved sedimentary fabric (units 610 and 630). Gravelly unit 640 is the first fill unit into the offset channel. Its basal contact forms one of the thalwegs used to measure channel offset (Fig. 5). Unit 640 is overlain by colluvial and/or pedogenically altered units 650 and 660, which are in turn cut by the channel that was subsequently filled by the coarse, angular, crudely bedded gravels in unit 670. In places, the texture of units 630 and 660 are indistinguishable, but the contact between them is well defined by a color contrast, with darker unit 660 above lighter units 630 and 610. Several ^{14}C samples were collected in trench T6′. However, only sample T6′-4 from the top of unit 630 yielded a reliable date that gives a maximum channel age (see Radiocarbon Dating section).

T8—First Downstream Channel

Coarse, angular, stratified gravels in units 840 and 870 with scour and fill structures are interpreted as channel fill deposits in trench T8 (Fig. 6d; Ⓔ supplemental Table 5 and Fig. 1b, available in the electronic edition of BSSA). The base of 840 is the offset thalweg we matched with that exposed in T6′ and T2. The channels were cut into units 810, 820, and 830, which are interpreted as colluvium. Unit 860 is a clayey silt deposit containing most of the radiocarbon-dated samples near its top. It could be either colluvium, washed down from adjacent hill slopes, or autochthonous alteration of channel deposits by bioturbation and other pe-

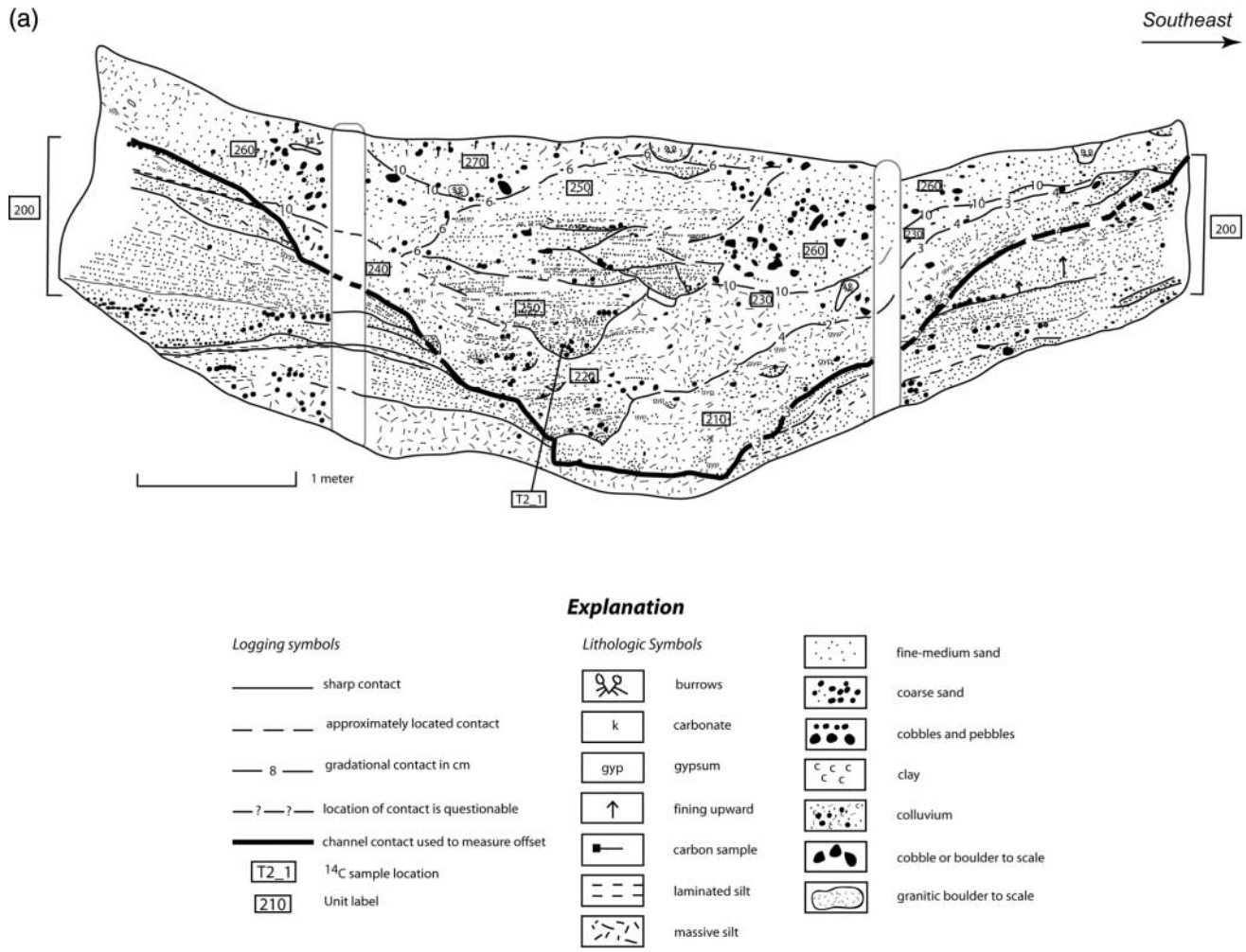

Figure 6. (a) Lithologic log of northeast wall of trench T2 (see Fig. 5 for location). Several nested channels are cut into the local Paso Robles bedrock unit. The channels are filled with clast-supported gravel that grade outward or are cut into and overlain by colluvial units or channel deposits that have been pedogenically altered. The lowermost channel thalweg (base of unit 210) is the match for the offset thalwegs exposed in T6′, T8, and T7. The explanation indicates the patterns, line types, and labels used in all of the logs. (*continued*)

dogenic processes. Most of the samples collected for dating were retrieved from this trench.

T7—Second Downstream Channel

Because of its older age, the stratigraphic relationships in trench T7 (Fig. 6e; Ⓔ supplemental Table 6 and Fig. 1c, available in the electronic edition of BSSA) are more obscured by pedogenesis than in the younger trenches. Nonetheless, unit 730 has eroded into the local bedrock (a Quaternary fan deposit) and its base represents the thalweg that we correlate with that exposed in trenches T2, T6′, and T8. This channel thalweg is offset about 48.8 m. Unit 740 is heavily pedogenically altered, but preserves a few channel gravel packages. Colluvial unit 750 dominates the upper portion of the exposure. Unit 760 has occasional disseminated lenses of coarse, angular-to-subangular sand and very fine angular pebble gravel within a more massive clayey, sandy silt. This unit most likely represents erosion and fill from the smaller watershed that the T7 channel has recently captured (Fig. 5).

Radiocarbon Dating

Carbonaceous samples collected from the excavations were large enough for radiocarbon dating and sufficiently numerous to provide age control for the units from which they were collected. Most of the samples dated were located in trenches T6′ and T8. Results of radiocarbon dating of samples most relevant to determination of slip rate are presented in Table 1. The median probability calibrated dates of samples are also displayed in Table 1 as a convenient summary of each sample.

Results for all samples are in supplemental Table 1,

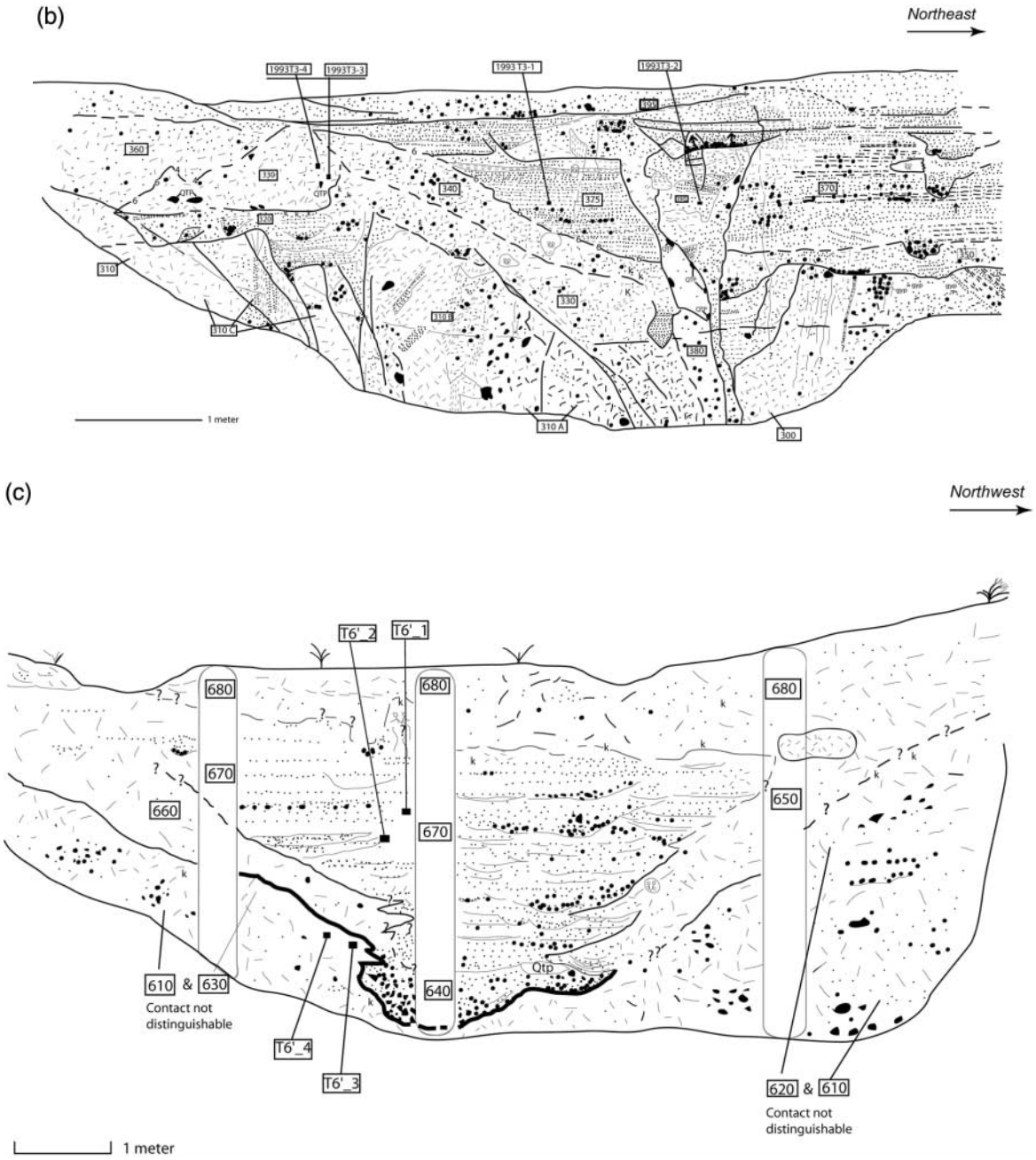

Figure 6. Continued. (b) Lithologic log of the northwest wall of trench T3 (see Fig. 5 for location). This trench exposed three main shear zones that progressively cut up section from southwest to northeast. Gray-green unit 300 is correlative with unit 200 from trench T2 (Fig. 6a) and is juxtaposed against highly sheared and deformed tan Paso Robles or older Quaternary units to the southwest. Units 370 and 375 represent the channel fill sequence. The two channel fill packages are separated by a fissure fill unit that probably formed in the 1857 earthquake. See the trench log explanation in Figure 6a. (c) Lithologic log of the southwest wall of trench T6 (Ⓔ see supplemental Fig. 1a, available in the electronic edition of BSSA, for the northeast wall and Fig. 5 for location). Clast-supported sand and gravel fluvial deposits fill nested channels cut at the base into local Plio-Quaternary bedrock (units 610 and 630). The base of unit 640 is the thalweg offset from the exposures in trench T2. Importantly, ^{14}C sample T6′-4 dates the colluvium into which the channel was cut, providing a maximum channel age. See the trench log explanation in Figure 6a. (*continued*)

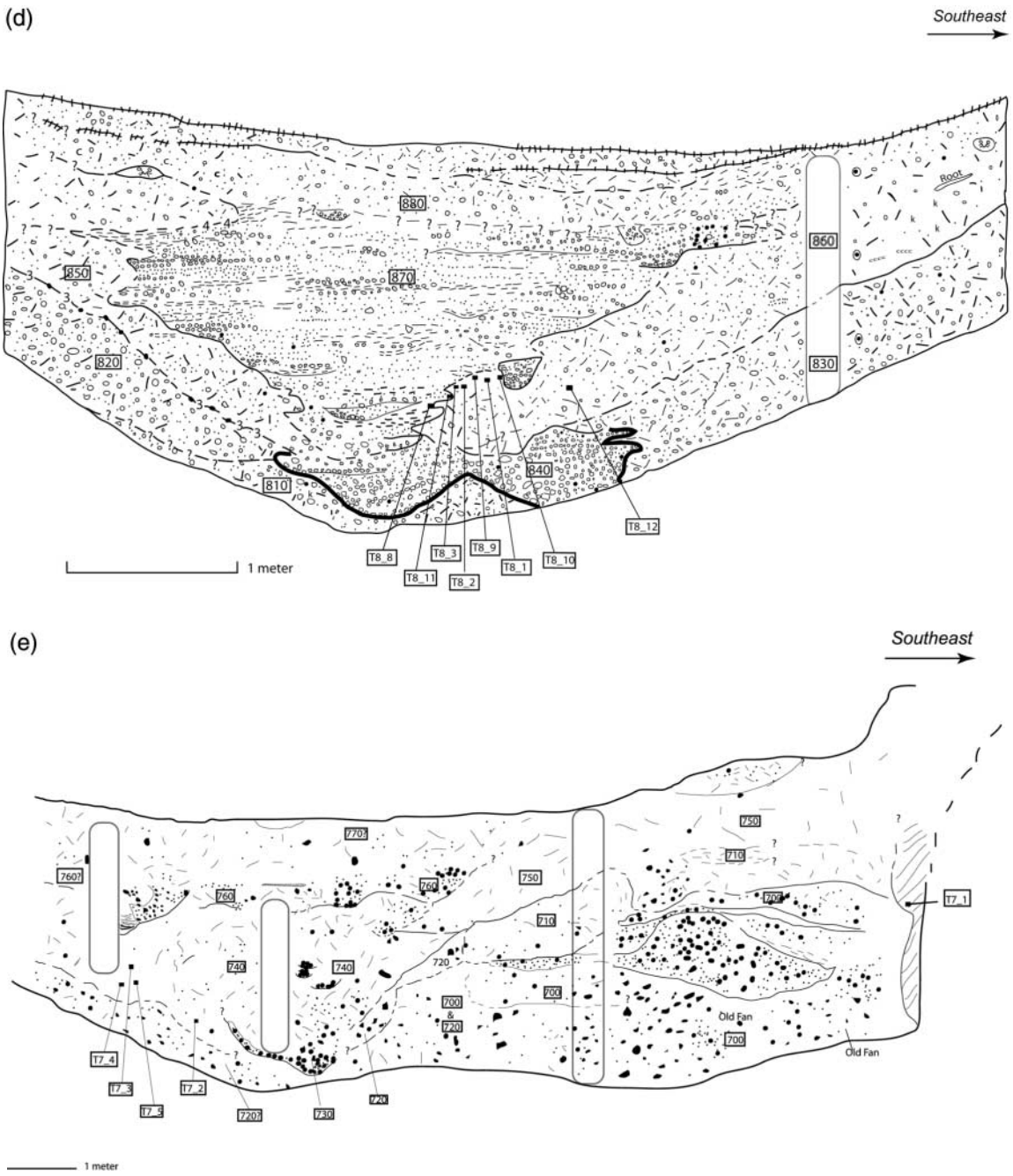

Figure 6. Continued. (d) Lithologic log of the northeast wall of trench T8 (Ⓔ see supplemental Fig. 1b, available in the electronic edition of BSSA, for the southwest wall and Fig. 5 for location). Clast-supported sand and gravel fluvial deposits fill nested channels cut at the base into local Plio-Quaternary bedrock (units 810 and 830). The base of unit 840 is the thalweg offset from the exposures in trench T2. Most of the ^{14}C samples in this study come from the top of unit 860 and provide a minimum channel age. See the trench log explanation in Figure 6a. (e) Lithologic log of the northeast wall of trench T7 (Ⓔ see supplemental Fig. 1c, available in the electronic edition of BSSA, for the southwest wall and Fig. 5 for location). Because of its older age, the stratigraphic relationships are more obscured than the younger trenches by pedogenesis. Nonetheless, unit 730 has eroded into the local bedrock (a Quaternary fan deposit) and its base represents the thalweg that we correlate with that exposed in trenches T2, T6′, and T8. This channel thalweg is offset about 48.8 m. See the trench log explanation in Figure 6a.

(Ⓔ available in the electronic edition of BSSA). Potential complications with age control in the Carrizo Plain include inherited age from detrital wood, the presence of shrubs that can live more than 800 years (Grant and Sieh, 1993) and anomalously old radiocarbon ages of terrestrial gastropods (Grant and Sieh, 1994). Three anomalously older dates were obtained from gastropod shells collected in trench T8 and from an undisturbed surface sample from outside the trenches.

The most relevant samples were collected from channel margin clayey silts (units 860 and 630) and channel fill deposits (unit 870) bounding the lower part of the channel margin in trenches T8 and T6′. None of the dated samples was indisputably collected from within the channel fill. Samples T8-8 and T8-11 were collected along a diffuse contact between channel fill (unit 870) and channel margin (unit 860). The older sample, T8-8 (Ⓔ supplemental Table 1, available in the electronic edition of BSSA) has a median probability date up to two centuries older than other samples from unit 860 and therefore is presumed to be reworked.

Constraint on the date of channel cutting or maximum age of channel offset is obtained from analysis of the dates and stratigraphic positions of samples shown in Table 1 and output from the program OxCal v. 3.10 (Bronk Ramsay, 1995, 2001). The stratigraphically lowest samples are T6′-3 (Ⓔ supplemental Table 1, available in the electronic edition of BSSA) and T6′-4 (Table 1). Sample T6′-3 is a millennium older than other samples, is presumed to be reworked, and therefore is not included in the analysis. Sample T8-11 was collected from the outermost channel fill, or the channel margin. The remaining samples in Table 1 were collected from within unit 860. An OxCal model was constructed to sum the cluster of seven samples from T8 and place samples T8-11 and T6′-4 in stratigraphic order. The results (Ⓔ supplemental Table 8, available in the electronic edition of BSSA) constrain the maximum age date of channel incision (A.D. 1160) to approximately the maximum age of sample T6′-4 (A.D. 1164; see Table 1).

Tectonic Geomorphology

The VMR site preserves a spectacular set of offset channels (Figs. 3–5). They drew the attention of Sieh (1977, 1978, 1979), who emphasized the study of channels 47–48 because they preserved the record of the last offset (8 ± 0.5 m). Channels 48, 46, and 45 were offset such that the penultimate offset of 7.5 ± 1 m could be estimated. Channel 44 is offset 27 ± 2.7 m according to Sieh (1977), and in combination with the other offsets at the site yields an offset in the third event back of about 10 ± 1 m. The offset history is interpretable because of the excellent preservation of the channels and because of the clear record of incision, offset, and abandonment (Fig. 3). However, the number of slip events that generated each offset cannot be determined directly from the geomorphology. Evidence from trench T3 indicates a minimum of three slip events contributed to the offset of Sieh's channel 44 (our study site). As described in the discussion, evidence from other studies suggests a maximum of five or six slip events.

The pattern of geomorphology and stratigraphy at VMR implied the following model by Sims *et al.* (1993; see also Sims, 1994) of tectonic offset and subsequent channel response: (1) a new channel is cut or inherited; (2) after initial offset, the channel may continue to incise; (3) continued offset and channel lengthening decreases local along-fault channel gradient, causing sedimentation as shingled, nested cut-in-fill channel deposits; and (4) further offset along the fault promotes increased deposition and filling of the channel. The filled channel may be capped by fan deposits and allow incision of a new channel across the fault or be captured by a topographic low juxtaposed by recurrent offset. Channel 44 is in this latter stage in its current configuration. There is little room in the channel for further deposition and it is likely to be abandoned soon (and will probably occupy a channel initially formed by channel 45; Figs. 3–5).

The geomorphology and stratigraphy in the channels reveal a record of filling by fluvial sedimentation, lateral colluviation, and pedogenesis. Typically, the channel units (e.g., 220, 250, 640, 670, 840, 870, 730, and 740) cut into or are overlain by reworked fluvial units (210, 230, 240, 260, 270, 650, 660, 680, 860, 880, 700–720, and 750). The older reworked fluvial units usually contain $CaCO_3$, which gives them a light color. In places, the basal boundary for the older colluvial units is diffuse (portions of T2) or sharp and scalloped (T9).

We have developed two end-member models for the development of the reworked fluvial units. In the first model the heavily bioturbated and pedogenically altered fluvial sediment no longer has sedimentary fabric preserved. This model is supported best by the relationships from T2 in which units 230 and 240 grade into the central channel unit 220 (Fig. 6a). In the second model colluvium is delivered to the channels during the relatively long periods of no fluvial transport in the channels. The colluvium shows interfingering relationships with the channel sediments. For example, T8 (Fig. 6d) has a wedge of colluvial material (unit 860) overlying the channel fill (unit 840), and is cut by unit 870.

The possibility of gullies, to the southeast of our study site, sourcing channels that would align with our gully is rejected by geomorphic and stratigraphic evidence. Strike-slip motion could have not have caused channel head 44 to line up with the older tails of channel 45 of our study and create an apparent offset. The displacement necessary to place the channel at this site location would be greater than the current acceptable displacement given the ages of the dated samples.

Offset Measurements

To measure the channel offsets, we surveyed the geomorphic trace of the SAF at VMR (N56°W) and projected the trench survey data that define the offset channel buried thalwegs to either be parallel or perpendicular to the trace.

The projection is also approximately parallel or perpendicular to the orientation of the trench walls. The distance along the fault versus elevation of the surveyed buried channel thalweg for the two walls of each trench (and topographic profile along the SAF through the trenches) is shown in the lower plot in Figure 5. The offset is measured as the relative distance between the lowest point in the T2 northeast channel thalweg and the thalweg centers (as we estimated represented by a given nail). We measured it for the pairs of buried offset channels in T2–T6′, T2–T8, T2–T7, and the associated geomorphic offsets from the surveyed topography. We did not make such a determination for T9 because evidence for an identifiable buried channel thalweg was ambiguous (Ⓔ see supplemental Fig. 1d, available in the electronic edition of BSSA).

Results of offset measurements from surveying are displayed in Table 2. The buried thalweg of the currently active channel is offset 24.8 m, with a qualitatively defined conservative measurement uncertainty of ±1 m. The geomorphic offset is 27.6 m. The geomorphic offset has significantly higher uncertainty because the geomorphic thalweg is broader and not as well defined as the buried thalweg.

The thalweg of the first beheaded channel that is exposed in T7 is offset 48.8 m with a geomorphic offset of 51.8 m. The geomorphic offset of the second beheaded channel that we tried to expose in T9 ranges from 71.9 to 79.0 m. There were no datable materials in trenches T7 and T9. As a result, only the downstream channel exposed by T6′ and T8 is used for slip-rate measurement.

Slip Rate

Slip rate is obtained from channel offset divided by time interval. The precision and accuracy of the slip rate depends on how accurately and precisely the measured parameters represent the actual tectonic offset of the channel. We measured offset of the buried thalweg, as exposed in the walls of trenches (24.8 m ± 1m), and as expressed by surficial geomorphology (27.6 m ± 1m). For slip-rate measurement, the buried thalweg is a better representation of channel offset because it is better defined morphologically and because it was formed at the time of initial channel incision. As described in the section on radiocarbon dating, the maximum age of sample T6′-4 (approx. A.D. 1160) provides a maximum age for incision of the channel, which postdates deposition of the sample.

Table 2
Offset Calculations

Wall	Offset (m)
T8NE	25.0
T8SW	25.5
T6′NE	24.4
T6′SW	24.4
Average	24.8
Geomorphic offset	27.6

The lowest surveyed point from T-6′ and T-8 was used to measure offset from lowest point of T-2. See Figure 5.

A minimum slip rate, 29.3 mm/yr, is derived from offset of the buried thalweg (24.8 m) divided by the maximum time interval (A.D. 2005–A.D. 1160). This scenario assumes that the channel was offset immediately following incision and uses the maximum possible date of incision as defined by sample T6′-4 and results of the OxCal model.

It is likely that some time passed between channel incision and offset. A faster slip rate can be derived based on the assumption that the channel was incised circa A.D. 1160 and offset by surface-rupturing "Event E" of Grant and Sieh (1994) dated A.D. 1218–1276. The shortest time interval of measurement would be the time between the youngest date of this event (A.D. 1276) and the 1857 earthquake. The resulting slip rate is 34.0 mm/yr. This slip rate is in excellent agreement with the late-Holocene slip rate of 33.9 ± 2.9 mm/yr measured at Wallace Creek (Sieh and Jahns, 1984).

A maximum slip rate can be derived from a shorter time interval. For example, the date of the most recent slip event, the 1857 earthquake, could be used as the end point of the time interval to obtain a slip rate of 35.6 mm/yr (i.e., 24.8 m/[A.D. 1857–A.D. 1160]). This slip rate also agrees well with Sieh and Jahns's (1984) late-Pleistocene measurement of ~36 mm/yr at Wallace Creek.

Discussion

This study fills a temporal gap between current deformation rates (Lisowski *et al.*, 1991; Argus and Gordon, 2001; Titus *et al.*, 2005) and older slip rates reported by Sieh and Jahns (1984). The minimum late-Holocene slip rate at VMR is 29.3 mm/yr and the maximum rate is 35.6 mm/yr, in excellent agreement with older rates reported at Wallace Creek. This result suggests that the slip rate has not changed measurably over the last few centuries to few millennia. The slip rate at VMR also provides insight into slip partitioning between the SAF in the Carrizo Plain and deformation in the Coast Ranges, as well as the degree of localization of faulting.

Figure 2 shows the SCEC Crustal Motion Model 3 (Shen *et al.*, 2003) from which we selected those velocities in a ~100-km-wide swath perpendicular to the SAF centered on the Carrizo Plain. We projected them to the N40°W direction to determine a velocity parallel to the average trace of the SAF northwest of the Transverse Ranges (note that projecting them to N56°W—local VMR SAF trace—only changes the gradient by 1–2 mm/yr). The N40°W velocity profile shows a steep gradient of about 30 mm/yr across the SAF at the Carrizo Plain. Assuming that these data represent steady interseismic motion, these data can be interpreted by calculating the surface-displacement profile from strike slip from the brittle–ductile transition zone (here assumed to be 12 km) to great depth (e.g., along an infinitely long vertical

screw dislocation; Thatcher, 1990). Two curves for 30 and 37 mm/yr of steady deep slip approximately bound the observed velocities in Figure 2. Further detailed analysis of these data is beyond the scope of this article, but clearly they are consistent with the slip rate we have determined. Importantly, the slip at the VMR site indicates that all of the regional shear of the SAF system in the area of the Carrizo Plain has been accommodated across a narrow, few-meter-wide fault zone for the last millennium.

If the deformation is so localized at the VMR site, an interesting question is how many surface ruptures generated the measured offset. Sieh (1978) proposed that the last three ruptures at VMR involved 8 ± 0.5 m, 7.5 ± 1 m, and 10 ± 1 m slip respectively, for a total offset of approximately 25 m. Detailed logging of trench T3 revealed evidence of at least three ruptures, but the total number of events could not be discriminated due to laterally discontinuous cut-and-fill channel stratigraphy. From extrapolation of findings at Wallace Creek (Liu *et al.*, 2004), the number of earthquakes could range from three to six. At Wallace Creek, displacement from the last five ruptures totaled 22.1 m. Therefore, at VMR the 24.8 ± 1 m offset of the buried thalweg could have been produced by five or six comparable ruptures, with an average dextral slip of 4 to 5 m each.

Acknowledgments

We would like to thank John Sims and John Hamilton of the U.S. Geological Survey (USGS) for sharing 1993 data and working with Arrowsmith to develop the site. We would also like to thank Mr. Leonard Bidart for granting us permission to work on Bidart Brothers property. Comments of J. Lienkaemper and an anonymous reviewer contributed substantially toward improving the manuscript. We are especially grateful for Lienkaemper's expert and specific advice about constructing an appropriate OxCal model. Thanks to the Keck Carbon Cycle AMS lab staff at UCI, and especially Drs. John Southon, Guaciara M. Dos Santos, and Susana E. Gonzalez for training and supervision. Nathan Toké, Kenneth Jones, Raymond Ludwig, and Frank Romaglia are thanked for help in the field, and Olaf Zielke for digitizing. Miryha Gould and Eric Runnerstrom produced images shown in Figure 3 from aerial photography and elevation data provided by Kerry Sieh. Thanks to Hector Hernandez for constant help, support, and constructive criticism. This project was supported by the USGS, Department of Interior, under USGS award 04HQGR0080, and by NSF EAR-0409500 and EAR-0409745 to Grant and Arrowsmith. Shoring was provided by the Southern California Earthquake Center (SCEC). The SCEC is funded by National Science Foundation (NSF) Cooperative Agreement EAR-0106924 and USGS Cooperative Agreement 02HQAG0008. The SCEC contribution number for this paper is 906.

References

Allen, C. R. (1968). The tectonic environments of seismically active and inactive areas along the San Andreas fault system, *Geological Sciences* **11,** 70–80.

Argus, D. F., and R. G. Gordon (2001). Present tectonic motion across the Coast Ranges and San Andreas fault system in central California, *Geol. Soc. Am. Bull.* **113,** no. 12, 1580–1592.

Bronk Ramsey, C. (1995). Radiocarbon calibration and analysis of stratigraphy: the OxCal program, *Radiocarbon* **37,** no. 2, 425–430.

Bronk Ramsey, C. (2001). Development of the radiocarbon program OxCal, *Radiocarbon* **43,** no. 2A, 355–363.

Dibblee, T. W., Jr. (1973). Regional geologic map of San Andreas and related faults in Carrizo Plain, Temblor, Caliente, and La Panza ranges and vicinity, California. U.S. Geol. Surv. Misc. Invest. Series Map I-757, scale 1:125,000.

Grant, L. B. (1996). Uncharacteristic earthquakes on the San Andreas fault, *Science* **272,** no. 5263, 826–827.

Grant, L. B., and A. Donnellan (1994). 1855 and 1991 surveys of the San Andreas fault: implications for fault mechanics, *Bull. Seism. Soc. Am.* **84,** no. 2, 241–246.

Grant, L. B., and K. Sieh (1993). Stratigraphic evidence for seven meters of dextral slip on the San Andreas fault during the 1857 earthquake in the Carrizo Plain, *Bull. Seism. Soc. Am.* **83,** 619–635.

Grant, L. B., and K. Sieh (1994). Paleoseismic evidence of clustered earthquakes on the San Andreas fault in the Carrizo Plain, California, *J. Geophys. Res.* **99,** no. B4, 6819–6841.

Lisowski, M., J. C. Savage, and W. H. Prescott (1991). The velocity field along the San fault in central and southern California, *J. Geophys. Res.* **96,** 8369–8389.

Liu, J. (2003). Slip behavior of the San Andreas fault through several earthquake cycles, *Ph.D. Thesis,* California Institute of Technology.

Liu, J., Y. Klinger, K. Sieh, and C. Rubin (2004). Six similar sequential ruptures of the San Andreas fault, Carrizo Plain, California, *Geology* **32,** no. 8, 649–652.

Prentice, C. S., and K. Sieh (1989). A paleoseismic site along the Carrizo segment of the San Andreas fault, central California, *EOS Trans. AGU* **70,** 1349.

Shen, Z. K., D. C. Agnew, R. W. King, D. Dong, T. A. Herrin, M. Wang, H. Johnson, G. Anderson, R. Nikolaidis, M. van Domselaar, K. W. Hudnut, and D. D. Jackson (2003). The SCEC crustal motion map, version 3.0, http://epicenter.usc.edu/cmm3/.

Sieh, K. E. (1977). Late Holocene displacement along the south-central reach of the San Andreas fault, *Ph.D. Thesis*, Stanford University.

Sieh, K. E. (1978). Slip along the San Andreas fault associated with the great 1857 earthquake, *Bull. Seism. Soc. Am.* **68,** 1731–1749.

Sieh, K. E. (1979). Geological studies of the Holocene behavior of the SAF, CA, *Proceedings of the International Research Conference on Intracontinental Earthquakes*, Ohrid, Yugoslavia.

Sieh, K. E., and R. H. Jahns (1984). Holocene activity of the San Andreas fault at Wallace Creek, California, *Geol. Soc. Am. Bull.* **95,** 883–896.

Sims, J. D. (1994). Stream channel offset and abandonment and a 200-year average recurrence interval of earthquakes on the San Andreas fault at Phelan Creeks, Carrizo Plain, California, in *Proceedings of the Workshop on Paleoseismology, U.S. Geol. Surv. Open-File Rept. 94-568*.

Sims, J. D., J. C. Hamilton, and R. Arrowsmith (1993). Geomorphic study of earthquake offsets and subsequent landform response along the San Andreas Fault, Carrizo Plain, California, *EOS Trans. AGU* **74,** 612.

Stuiver, M., P. J. Reimer, E. Bard, J. W. Beck, G. S. Burr, K. A. Hughen, B. Kromer, F. G. McCormac, J. V. D. Plight, and M. Spurk (1998). INTCAL98 radiocarbon age calibration 24,000–0 BP, *Radiocarbon* **40,** 1041–1083.

Stuiver, M., and H. A. Polach (1977). Discussion; reporting of C-14 data, *Radiocarbon* **13,** no. 3, 355–363.

Thatcher, W. (1990). Present-day crustal movements and the mechanics of cyclic deformation, in *The San Andreas Fault System, California*, R. E. Wallace (Editor), *U.S. Geol. Surv. Profess. Paper 1515*, 189–205.

Titus, S. J., C. DeMets, and B. Tikoff (2005). New slip rate estimates for the creeping segment of the San Andreas fault, California, *Geology* **33,** 205–208.

Vedder, J. G., and R. E. Wallace (1970). Map showing recently active breaks along the San Andreas and related faults between Cholame Valley and Tejon Pass, California, U.S. Geol. Surv. Map I-574, scale 1:24,000.

Wells, D. L., and K. J. Coppersmith (1994). New Empirical relationships among magnitude, rupture length, rupture area, and surface displacement, *Bull. Seism. Soc. Am.* **84,** 974–1002.

Working Group on California Earthquake Probabilities (WGCEP) (1988). Probabilities of large earthquakes occurring in California on the San Andreas Fault, *U.S. Geol. Surv. Open-File Rept. 88-398*.

Working Group on California Earthquake Probabilities (WGCEP) (1995). Seismic hazards in southern California: probable earthquakes, 1994–2024, *Bull. Seism. Soc. Am.* **85,** 379–439.

University of California, Irvine
Department of Environmental Health, Science and Policy
Irvine, California 92697-7070
(G.R.N., L.B.G.)

Arizona State University
Department of Geological Sciences
Tempe, Arizona 85287-1404
(J R.A., J.J.Y.)

Manuscript received 12 May 2005.